Observation of the Talbot effect from a surface-acoustic-wave dynamic grating

Fisicaro, M.; Doedes, Y.C.; Steenbergen, T.A.; Exter, M.P. van; Löffler, W.

Observation of the Talbot effect from a surface-acoustic-wave dynamic grating

M. Fisicaro,* Y. C. Doedes, T. A. Steenbergen, M. P. van Exter, and W. Löffler
Leiden Institute of Physics, Leiden University, P.O. Box 9504, 2300 RA Leiden, Netherlands

(Received 11 November 2024; revised 28 January 2025; accepted 20 March 2025; published 9 April 2025)

We demonstrate the dynamical Talbot effect caused by optical diffraction from standing surface acoustic waves (SAWs). The Talbot effect is a wave interference phenomenon in the Fresnel regime, and we observe it with a fiber-based scanning optical interferometer on a SAW Fabry-Perot cavity. By studying the interferometric signal at 1 GHz, next to the usual phase term we discover the existence of an amplitude-modulated term which vanishes at periodic positions when we displace the acoustic device relative to the beam focus. With this, we reveal the optical Talbot effect where, despite the curved wavefronts of the optical field, the conventional Talbot length appears. Finally, we propose to use the amplitude modulation as a different way of imaging surface acoustic waves.

DOI: 10.1103/PhysRevA.111.043513

I. INTRODUCTION

Diffraction and interference of light is a well-known phenomenon that arises from its wave nature, resulting in many fascinating effects, from the Arago spot [1] to modern ptychography [2–4]. Of particular interest is the Talbot effect, where diffraction of a plane wave by a periodic structure, such as a grating, results in periodic images of the grating at specific distances. This phenomenon is also referred to as lensless or self-imaging because it allows the reconstruction of images without the use of lenses [5–7]. It was first discovered in optics in 1836 by Talbot [8], but it was Lord Rayleigh who quantitatively explained it in 1881 [9]. Four years later, Lord Rayleigh also predicted the existence of a particular type of acoustic surface waves, characterized by an elliptical motion of the surface [10]. He accurately envisioned that these waves have a significant role in earthquakes and elastic solids, and they were later named Rayleigh waves. Even though the Talbot effect has been observed in many different systems [11–17], to the best of our knowledge, it has never been observed as a consequence of optical diffraction from Rayleigh waves.

This particular type of surface acoustic waves (SAWs) can be excited using an interdigital transducer (IDT) [18–20] on the surface of a piezoelectric substrate at frequencies up to a few GHz, which, for most materials, corresponds to acoustic wavelengths down to the submicrometer range [21–24]. If confined in an acoustic Fabry-Perot cavity [25–32], standing SAWs appear, resulting in an oscillating surface grating, which can dynamically diffract an optical beam upon reflection by spatial phase modulation. In our case, we use a fiber-based scanning optical Michelson interferometer to image the displacement generated by 1 GHz SAWs. For spatially resolved interferometric imaging of the SAWs shown in Fig. 1, this diffraction is an, in principle, unwanted but unavoidable effect since, at this frequency, the acoustical wavelength $\Lambda = 2.8$ μm and the beam spot size of the focused laser beam $2w_0 = 2.8$ μm (for $\lambda = 980$ nm and 0.55 NA) are comparable in size. In our experiment, we were originally interested in the optical phase modulation induced by the SAWs, but we found that the interferometric signal consists of both a phase-modulation term and an amplitude-modulation term that appears due to mode filtering by the single-mode optical fiber. In this study, we theoretically and experimentally show that the amplitude-modulation term can be significant, enabling a simpler way of measuring SAWs, and we report the observation of the Talbot effect from a standing SAW grating, sketched in Fig. 1.

II. EXPERIMENT

Our experimental setup, shown in Fig. 2, is a Michelson interferometer implemented with a polarization-maintaining single-mode fiber coupler as the beam splitter (PM BS). Narrow linewidth laser light of wavelength $\lambda = 980$ nm, after optical isolation, enters the fiber coupler through port A and is split into the sample (D) and reference arm (C). In the reference arm, the light is focused onto a mirror by a single aspheric lens and back-reflected into the fiber. In the sample arm (D), the light is first collimated and then strongly focused onto the GaAs-based SAW device with an aspheric lens with 0.55 NA, resulting in $w_0 = 1.4$ μm, and the back-reflected light is coupled back into the same single-mode fiber. Both light fields are combined in the polarization-maintaining splitter and detected by a slow photodiode and a fast photodiode. The signal on the slow photodiode is used to stabilize the interferometer by controlling the length of the reference arm with a piezo driven by a proportional-integral-derivative (PID) controller. The signal on the fast photodiode corresponds to the SAW oscillations and is measured with a gigahertz lock-in amplifier which can detect both amplitude and phase. The same lock-in amplifier is used to drive the SAW device. The SAW device is a surface-acoustic-wave (SAW) Fabry-Perot cavity fabricated on a GaAs substrate, where SAWs are excited by an

*Contact author: fisicaro@physics.leidenuniv.nl

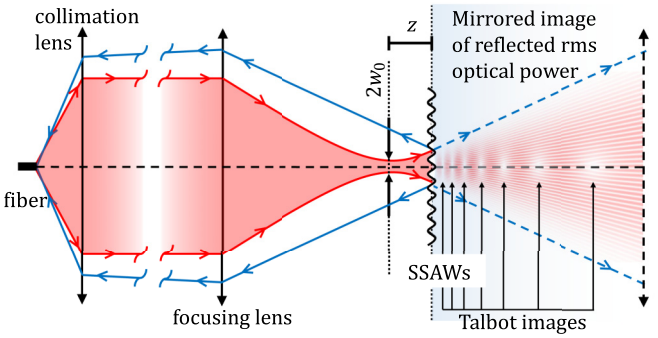

FIG. 1. Sketch of the experiment: Laser light from a single-mode fiber is first collimated and then focused onto a partially reflecting surface on which standing surface acoustic waves (SSAWs) are excited. The incident light is reflected back; for clarity, we plot its mirrored image to the right of the reflecting surface. If the position of the beam waist z is displaced with respect to the reflecting surface, the light beam illuminates multiple periods of the oscillating surface grating and the Talbot effect occurs. The self-images of the field at the grating, produced by the Talbot effect, are visible as regions of zero power on the right of the grating, where we have plotted the rms optical power of the reflected diffracted beam.

interdigital transducer with 10 finger pairs inside the resonator; see inset in Fig. 3. The SAW mirrors are implemented as short-circuited metal gratings with 250 elements each, 50 nm thick. The device is designed for a frequency of 1 GHz corresponding to a SAW wavelength of $\Lambda = 2.8$ μm. The SAW device is mounted on a three-axis nanopositioning stage in the sample arm of the interferometer, where translation along the optical (z) axis allows one to adjust the focus of the laser beam, while the x and y axes allow us to scan the laser focus over the SAW device, in order to reconstruct an image of the out-of-plane displacement of the SAWs. For a more complete description of the experimental setup, see [33]. While our setup uses lock-in detection and can measure the

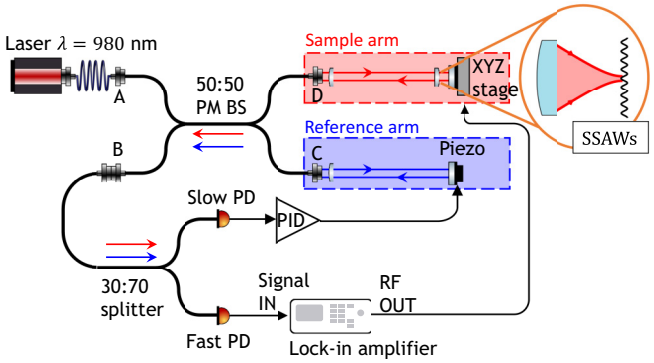

FIG. 2. Scheme of the fiber-based Michelson interferometer used in our experiment. Laser light is split into two different optical paths: the sample arm (red) where the light is reflected off of a surface acoustic wave device, and the reference arm (blue) where the arm is reflected off of a piezo-actuated mirror. The light from these two optical paths is recombined and is detected by a fast photodiode (fast PD), generating a gigahertz signal that is then measured with a lock-in amplifier. The same lock-in amplifier also drives the surface-acoustic-wave device at the frequency of 1 GHz.

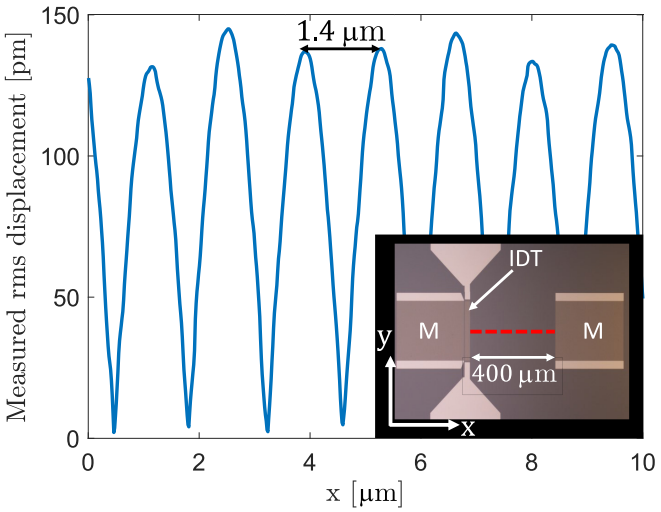

FIG. 3. Microscope image (inset) of the SAW cavity showing the IDT and the SAW mirrors (M), and standing wave pattern measured along a short section of the dashed red line. This is an interferometric measurement obtained by allowing light both in the reference and sample arm of the interferometer. It shows the expected periodicity of $\Lambda/2 = 1.4$ μm, with an rms surface displacement of ∼140 pm at the antinodes.

amplitude and phase of the surface displacement, in this work we only consider the amplitude of the measured SAW displacement. In Fig. 3, we show an amplitude measurement of the root-mean-square (rms) standing SAW displacement, taken along the dotted red line visible in the microscope picture of the SAW device (inset). This measurement is taken with the device in focus ($z = 0$) and it is interferometric since we are using both arms of the interferometer. However, we have found that also with a blocked reference arm, under the right circumstances, the SAW signal appears very clearly. This originates from a complicated form of periodic focusing and defocusing of the reflected beam, which modulates its collection efficiency in the single-mode fiber. We call the signal in the conventional case the *interferometric signal*, and if the reference arm is blocked, the *amplitude modulation*. We will now develop a theoretical model explaining this effect; importantly, we not only consider the case that the SAW device is in focus, but at a distance z from focus (Fig. 1).

Since we use throughout the setup linearly polarized light, it is sufficient to use scalar fields for the input field E_{in}, the collected field E_{col}, and the reference field E_{ref}. We introduce the complex collection ratio

$$\alpha(t) = \frac{E_{\text{col}}(t)}{E_{\text{in}}}, \tag{1}$$

which is a measure of the amplitude and phase of the reflected light collected by the single-mode fiber, relative to the input light that enters the sample arm of the interferometer. Once we know $\alpha(t)$, we can write the total intensity at the fast photodiode as

$$\begin{aligned} I_{\text{tot}} &= |E_{\text{ref}} + \alpha(t)\, E_{\text{in}}|^2 \\ &= I_{\text{ref}} + |\alpha(t)|^2 I_{\text{in}} + \text{Re}[2\alpha(t) E_{\text{in}} E_{\text{ref}}^*], \end{aligned} \tag{2}$$

where Re denotes the real part. We also note that while phase variations in $\alpha(t)$ are only visible in the double product term of Eq. (2), amplitude variations are also visible in the $|\alpha(t)|^2 I_{\text{in}}$ term and can also be observed with the blocked reference arm when $E_{\text{ref}} = 0$.

The calculation of the complex collection ratio $\alpha(t)$ is based on the overlap integral between the Gaussian mode supported by the fiber and the beam reflected by the SAW device, as a function of the defocusing, namely, the distance z between the SAW device surface and the beam-waist position of the focused Gaussian beam. This overlap integral can be calculated at any plane; for simplicity, we choose to calculate it on the device surface.

Due to the presence of standing SAWs along the x axis, we can model the surface out-of-plane displacement as

$$\Delta d(x, y, t) = A(t)\ \cos\left[K(x - x_0)\right], \tag{3}$$

where $K = 2\pi/\Lambda$ is the SAW wave number, x_0 is the transverse distance between the center of the laser focus and the position of the standing SAW antinode, and $A(t) = A_0 \cos(\Omega t)$ is the time-dependent amplitude of the SAW with angular frequency Ω and peak displacement A_0. There is no dependency on y because the standing SAW are excited only along the x axis. In Eq. (1), we defined the complex collection ratio as a function of time, but now we compute it also as a function of z and x_0: $\alpha(t) \to \alpha(z, x_0, t)$. From the calculations shown in Appendix A, we obtain

$$\begin{aligned}
\alpha(z, x_0, t) &= \alpha_{\text{DC}}(z) + \alpha_{\text{AC}}(z, x_0)\ \cos(\Omega t), \\
\alpha_{\text{DC}}(z) &= \frac{1}{1 + i\tilde{z}}, \\
\alpha_{\text{AC}}(z, x_0) &= \frac{2ikA_0 \cos(Kx_0) \times \exp\left[-B(1 - i\tilde{z})\right]}{1 + i\tilde{z}}.
\end{aligned} \tag{4}$$

Here, $\tilde{z} = z/z_R$, $z_R = \pi w_0^2/\lambda$ is the Rayleigh range of the focused Gaussian beam, w_0 is its waist radius, $k = 2\pi/\lambda$ is the wave number, and $B = K^2 w_0^2/8$. The complex collection ratio $\alpha(z, x_0, t)$ can be separated into two parts: a static term $\alpha_{\text{DC}}(z)$, which is a Lorentzian function of z and describes the complex collection ratio in the absence of standing SAWs, and a dynamic term $\alpha_{\text{AC}}(z, x_0)$, which describes the effect of the time modulation of the light field by the standing SAWs. This dynamic term not only contains the Lorentzian attenuation as a function of the defocusing, but also an additional exponential term that depends on the ratio between the Gaussian waist radius w_0 and the acoustic wavelength Λ via B. This exponent B is a complex number, meaning that $\alpha_{\text{AC}}(z, t)$ has a certain periodicity in z.

III. ONE-BEAM EXPERIMENT

Here we block the reference arm, so that the signal is only given by the amplitude modulation. The quantity responsible for the amplitude modulation is $|\alpha(z, x_0, t)|^2$, which contains a DC component and components at frequencies Ω and 2Ω. In our experiment, we are only interested in the Ω component since the AC-coupled RF photodiode blocks the DC component, and the lock-in amplifier demodulates at Ω. Moreover, the 2Ω term is much smaller in amplitude than the Ω term since it scales like A_0^2, as opposed to A_0, for the Ω term. After the demodulation by the lock-in amplifier, we are left with an rms signal of the amplitude modulation given by

$$V_{\text{amp}}^{\text{rms}}(z)\ \propto\ \frac{2|\gamma|e^{-B}}{\sqrt{2}(1 + \tilde{z}^2)} \times |\sin(B\tilde{z})|, \tag{5}$$

where $\gamma = 2kA_0 \cos(Kx_0)$ and the proportionality symbol means that we are not taking into account the gain provided by the photodiode and lock-in amplifier. This equation gives periodic zeros at positions that solve the equation $\sin(B\tilde{z}) = 0$. Substituting $B = K^2 w_0^2/8 = \pi^2 w_0^2/(2\Lambda^2)$ and $\tilde{z} = z\lambda/(\pi w_0^2)$, we find that the positions of the zeros are given by $z = n \times z_T$, where n is an integer and $z_T = 2\Lambda^2/\lambda$ is the conventional Talbot length for a diffraction grating with period Λ illuminated by a plane wave.

IV. TWO-BEAM EXPERIMENT

Here, light from the sample arm interferes with light from the reference arm. These two light beams are adjusted to have equal intensities at zero defocusing ($z = 0$), meaning $I_{\text{ref}} = I_{\text{in}}$ in Eq. (2). We lock the interferometer at the side of the fringe, such that the total intensity of the interfering beams is $I_{\text{lock}} = 2I_{\text{ref}}$, which corresponds to the light in the reference arm having phase $\phi_{\text{ref}} = \pm\pi/2$ for $z = 0$. If now we introduce a defocusing ($z \neq 0$), α_{DC} changes both in amplitude and in phase, lowering the light intensity from the sample arm. Consequently ϕ_{ref} also changes to keep the interferometer locked. While we can calculate $\phi_{\text{ref}}(z)$ from Eq. (2), imposing that $I_{\text{tot}} = I_{\text{lock}}$, a more useful quantity is the difference between the phase of $\alpha_{\text{DC}}(z)$ and the phase of the reference beam, $\Delta\phi(z) = \arg[\alpha_{\text{DC}}(z)] - \phi_{\text{ref}}(z)$,

$$\Delta\phi(z) \simeq \mp\text{acos}\left(\frac{\tilde{z}^2}{2\sqrt{1 + \tilde{z}^2}}\right), \tag{6}$$

which depends on whether we lock the interferometer on a positive ($-$) or negative ($+$) slope. We note that in the derivation of this equation, we considered $\arg(\alpha_{\text{DC}}) \simeq \arg(\alpha)_{\text{DC}}$ and $|\alpha_{\text{DC}}| \simeq |\alpha|_{\text{DC}}$, which is allowed since the SAW displacement is very small. The rms of the total interferometric signal is obtained by calculating the rms value of the Ω component of Eq. (2), which for small SAW displacement A_0 can be approximated as

$$V_{\text{tot}}^{\text{rms}}(z) \simeq \frac{2|\gamma|e^{-B}}{\sqrt{2}}\left|\frac{\sin(\Delta\phi + B\tilde{z})}{\sqrt{1 + \tilde{z}^2}} + \frac{\sin(B\tilde{z})}{1 + \tilde{z}^2}\right|. \tag{7}$$

The first term in the modulus is from the phase modulation, while the second term originates from the amplitude modulation. In detection, the phase-modulation term cannot be separated from the amplitude-modulation term, as it is the result of interference. In mathematical terms, $V_{\text{tot}}^{\text{rms}} \neq V_{\text{amp}}^{\text{rms}} + V_{\text{phase}}^{\text{rms}}$ due to the nonlinearity of the modulus function.

V. DISCUSSION

Now we compare our theory to experiments where we measure both the amplitude modulation $V_{\text{amp}}^{\text{rms}}$ and the total interferometric signal $V_{\text{tot}}^{\text{rms}}$ as a function of the defocusing distance z. In particular, we show the results corresponding to the situation where the focused Gaussian beam is centered on an antinode of the standing SAW, corresponding to $x_0 = 0$

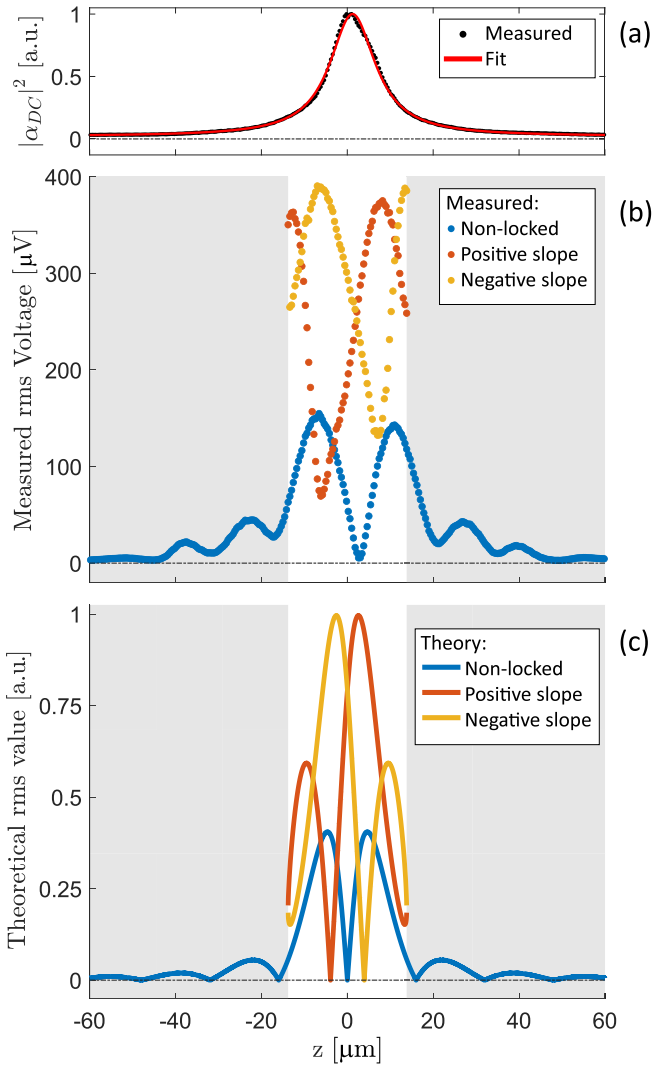

FIG. 4. (a) The measured DC component of the complex collection ratio (black) as a function of the defocusing z, with the corresponding fit (red). (b) Experimental and (c) theoretical Ω component of the amplitude modulation (blue) and of the total interferometric signals for the interferometer locked at the positive (red) or negative (yellow) slope.

in Eqs. (5) and (7). While changing the defocusing z, the relative position x_0 between the antinode and the beam spot could change due to imperfect alignment. To compensate for this, we do a short line scan along the x direction, exemplarily shown in Fig. 3, and we average the amplitudes of the measured peak values. In Fig. 4(a), we show the measured DC coupling ($|\alpha_{\mathrm{DC}}|^2$) as a function of z (black) and the corresponding Lorentzian fit (red). We fit the data with a modified version of $|\alpha_{\mathrm{DC}}|^2$ introduced in Eq. (4), to allow for an offset in intensity and in the defocusing. From the fit, the offset in the defocusing is $z_0 = 1.22$ μm. Figure 4(b) shows the measured amplitude modulation $V_{\mathrm{amp}}^{\mathrm{rms}}$ in blue, as well as the total interferometric signals $V_{\mathrm{tot}}^{\mathrm{rms}}$, obtained by locking the interferometer on the positive (red) or negative (yellow) slope. The measured signal is the rms voltage detected by the lock-in amplifier after 1 GHz demodulation. The gray areas are regions where it is not possible to lock the interferometer due to a decrease in the light intensity coupled back to the fiber in the sample arm of the interferometer. Figure 4(c) shows the corresponding theoretical data based on Eqs. (5)–(7).

We observe excellent qualitative agreement between measurements and theory: the signals are almost symmetric with respect to the z defocusing, the total interferometric signals locked at a positive and negative slope intersect at the defocusing z for which the amplitude modulation is zero, and the positions of the minima in the amplitude modulation are close to periodic with period $z_{\mathrm{period}} = (15.6 \pm 2.8)$ μm. This value is close to the expected periodicity from Eq. (5): $z_T = 2\Lambda^2/\lambda = 16$ μm. However, some quantitative discrepancies remain. For instance, the ∼3 μm offset in the amplitude modulation relative to $z = 0$ arises from improper alignment, particularly in locating the laser focus. We determined $z = 0$ by monitoring the reflected beam on a CCD camera (not shown in Fig. 2), minimizing the laser spot size and maximizing the DC coupling to the fiber by adjusting the alignment optics (also not shown in Fig. 2). Given the many degrees of freedom in the alignment optics, the maximum coupling that is achieved may correspond to a local rather than a global maximum, as suggested by the slightly asymmetric DC coupling in Fig. 4(a). In hindsight, a better alignment procedure to locate the laser focus would be simultaneously minimizing the 1 GHz amplitude-modulation signal, while maximizing the DC coupling. Additionally, the nonzero minima and asymmetry in the peak heights between negative and positive defocusing are attributed to spurious reflections inside the fiber beam splitter, as qualitatively confirmed by simulations.

VI. TALBOT EFFECT

We have seen from Eq. (5) that the amplitude modulation is periodic in z with the period $z_T = 2\Lambda^2/\lambda$. To simplify the following math, we now define a new coordinate system $\bar{z}$, with the SAW device placed at the origin $\bar{z} = 0$, and the beam focus at position $\bar{z} = z$. For clarity, we unfold the back-reflected light propagation to the right of $\bar{z} = 0$, as shown in Fig. 5. In this new coordinate system and due to the symmetric unfolding with respect to $\bar{z} = 0$, the projected image of the fiber is always at position $\bar{z} = -z$, and the field coupled back to the fiber after reflection is the field at this position mode-matched to the fiber. Since we know the optical field at the grating plane $\bar{z} = 0$, we can propagate it to $\bar{z} = -z$ using the Fresnel-Kirchhoff diffraction integral; the detailed calculation is shown in Appendix B. In Fig. 5(a), we show the intensity of the propagated light field after reflection from the grating. Contrary to the case of a grating illuminated by a plane wave, under Gaussian beam illumination, the Talbot self-images are laterally magnified by a factor $M_G = R_{\bar{z}}/(R_{\bar{z}} - \bar{z})$ [34], where $R_{\bar{z}} = (\bar{z} - z) \times [1 + z_R^2/(\bar{z} - z)^2]$ is the radius of curvature of the Gaussian beam at a generic observation plane $\bar{z}$. Also the positions of the self-images are nonperiodic in $\bar{z}$ and given by solutions to [34]

$$m\frac{z_T}{2} = \frac{R_{\bar{z}} - \bar{z}}{R_{\bar{z}}} \times \bar{z}, \tag{8}$$

where m is a positive integer.

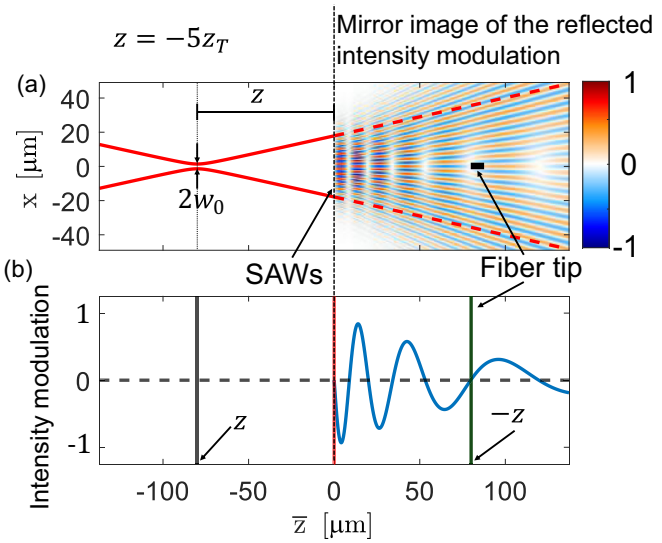

FIG. 5. Example of Talbot pattern obtained with a beam defocusing of $z = -5z_T$. (a) In the half plane $\bar{z} < 0$, a plot of the Gaussian beam before the grating. In the half plane $\bar{z} > 0$, a plot of the mirrored image of the reflected light-intensity modulation, after subtracting the constant intensity of the nondiffracted Gaussian beam. We considered a SAW profile given by Eq. (3), for $x_0 = 0$ and $t = 0$. Self-images of the field at the grating appear at specific positions given by Eq. (8), here visible as zones with zero-intensity modulation. (b) Cross-sectional plot of (a) along $x = 0$ showing that on the optical axis, the intensity modulation of the reflected field is zero at the positions of the self-images, and in particular at the mirrored position of the image of the fiber tip as indicated.

Combining all this, we find that remarkably, when the beam focus is at a distance $z = n \times z_T$ from the grating, with n an integer number, there is always one of the magnified Talbot self-images at the position $\bar{z} = -z$, coinciding with the position of the fiber and shown for $n = 5$ in Fig. 5(a). Again, because the surface motion does not give a Ω signal if it is in focus, also at these Talbot replica positions, the amplitude-modulation signal vanishes.

In Fig. 5(a), we can also observe that the region of constant intensities is concentrated close to the optical axis ($x = 0$); this is because we are illuminating only a small portion of the grating. We note that the number of self-images obtained after reflection depends on the Gaussian beam radius at the grating, and therefore on the number of grating periods that are illuminated. In particular, the minimum beam radius needed to observe a number m of self-images is given by (see Appendix B)

$$w_{\min}(m) = \Lambda\sqrt{\frac{2m}{\pi}}. \tag{9}$$

VII. CONCLUSIONS

By using a fiber-based Michelson interferometer to measure GHz standing SAWs in a SAW device, we discovered that on top of the usual phase-modulation term, the total interferometric signal also has a significant amplitude-modulation term. We showed that the amplitude modulation vanishes not only if the device is in focus, but also at periodic defocusings from the SAW device, corresponding to multiples of the Talbot length. This is explained by a combined change of the radius of curvature and the Talbot effect for curved wavefronts [34]. Our findings also show that an interferometric setup is not always the optimal solution for measuring spatially resolved oscillating surface displacements. Simple amplitude measurements with a single-mode fiber can be an easier way and the fiber splitter can be replaced by a fiber circulator. Our theory shows that in this case, the GHz signal can exceed the one obtained with an interferometer if the SAW period Λ is smaller than the beam waist: $\Lambda \lesssim w_0$, as shown in Appendix C. This is highly relevant in 5G telecommunication technology and the emerging field of quantum acoustics [26], where SAW devices operate at several gigahertz. In these contexts, the high frequencies involved correspond to submicrometer acoustic wavelengths—smaller than the conventionally achievable laser beam spot sizes. Under these conditions, our method enhances the detection signal of surface displacement, enabling a more sensitive optical characterization of SAW devices.

ACKNOWLEDGMENTS

We acknowledge funding from a NWO Vrij Programma Grant No. QUAKE, 680.92.18.04, the European Union's Horizon 2020 research and innovation programme under Grant Agreement No. 862035 (QLUSTER), and the Quantum Software Consortium.

APPENDIX A: THE COMPLEX COLLECTION RATIO

Here we derive the complex collection ratio $\alpha(z, x_0, t)$. We use the shifted reference frame where the focus of the Gaussian beam, as the projected image of the input fiber, is the origin of the optical axis, and the reflecting surface is at a distance z. This shift does not change the final results that depend only on the relative distance between the SAW device and the focus of the Gaussian beam. We consider the ideal case where the imaging system produces a perfect image of the fiber tip in the focus. This field can be written as $E_{\text{in}}(x, y, z, t) = \psi^+_{\text{in}}(x, y, z)\ \exp(-ikz + i\omega t)$ with a forward-propagating Gaussian mode (without Gouy phase),

$$\begin{aligned}\psi^+_{\text{in}}(x, y, z) &= \frac{\sqrt{2}}{\sqrt{\pi}w(z)} \times \exp\left[-ik\frac{x^2 + y^2}{2q(z)}\right] \\ &= \frac{\sqrt{2}}{\sqrt{\pi}w(z)} \times \exp\left[-\frac{x^2 + y^2}{w^2(z)}(1 + i\tilde{z})\right], \end{aligned} \tag{A1}$$

where $q(z) = z + iz_R$ is the complex beam parameter, $z_R = \pi w_0^2/\lambda$ is the Rayleigh range, w_0 is the beam-waist radius located at $z = 0$, $w(z) = w_0\sqrt{1 + \tilde{z}^2}$ is the beam radius at position z, and $\tilde{z} = z/z_R$. The field is normalized,

$$\iint |\psi^+_{\text{in}}(x, y, z)|^2\, dx\, dy = 1. \tag{A2}$$

The complex collection ratio defined in the main text can be calculated via the overlap integral between the reflected backward-propagating field and the backward-propagating image of the input field $\psi^-_{\text{in}} = (\psi^+_{\text{in}})^*$. This overlap integral can be calculated at any z plane since optical propagation

is a unitary operation. We calculate it at the plane of the SAW device. For a flat and perfectly reflecting interface, the reflected field mimics the input field $E^-_{\text{refl}} = E_{\text{in}}$, and we obtain the DC coupling,

$$\alpha_{\text{DC}} = e^{2ikz} \iint \psi^+_{\text{in}}(x, y, z)^2 \, dx \, dy = \frac{e^{2ikz}}{1 + i\tilde{z}}.$$

We can calculate the in-coupling efficiency η as

$$\eta = |\alpha_{\text{DC}}|^2 = \frac{I_{\text{col}}}{I_{\text{in}}} = \frac{1}{1 + \tilde{z}^2}, \tag{A3}$$

which corresponds to the DC coupling when we displace the reflecting surface by an amount z, with respect to the position of the beam waist.

We now consider how standing surface acoustic waves (SAWs) modulate the complex collection ratio α. In the presence of standing SAWs, the reflecting surface oscillates with the profile

$$\Delta z(x, y) = A(t) \, \cos[K(x - x_0)], \tag{A4}$$

where $K = 2\pi/\Lambda$ is the SAW wave number, Λ is the SAW wavelength, $A(t) = A_0 \, \cos(\Omega t)$ is the displacement at an antinode with amplitude A_0, Ω is the SAW angular frequency, and x_0 indicates the position of the laser beam. The reflected field becomes

$$E^-_{\text{refl}} = \exp(2ik\Delta z) E_{\text{in}}, \tag{A5}$$

where $\Delta z > 0$ is away from the input fiber. From Eq. (A5), we remove the stationary phase factor $\exp(2ikz)$, and we obtain

$$\alpha(z, x_0, t) = \iint \exp(2ik\Delta z) \psi^+(x, y, z)^2 \, dx \, dy. \tag{A6}$$

Substituting (A4) into (A6), we arrive at the following integral:

$$\alpha(z, x_0, t) = \iint \exp\{2ikA(t) \cos[K(x - x_0)]\} \times \exp\left[-\frac{2(x^2 + y^2)(1 + i\tilde{z})}{w^2(z)}\right] \frac{dx \, dy}{\pi w^2(z)}. \tag{A7}$$

This integral can be solved by separating the integral in the x and y directions,

$$\alpha(z, x_0, t) = \frac{2}{\pi w^2(z)} I_y \, I_x, \quad \text{where}$$
$$I_y = \int_{-\infty}^{+\infty} \exp\left[-\frac{2y^2}{w^2(z)}(1 + i\tilde{z})\right] dy,$$
$$I_x = \int_{-\infty}^{+\infty} \exp\left[-\frac{2x^2}{w^2(z)}(1 + i\tilde{z})\right] \times e^{2ik\Delta z} \, dx. \tag{A8}$$

I_x and I_y can be solved by using the standard integral,

$$\int_{-\infty}^{+\infty} \exp[-ax^2 + ibx] \, dx = \sqrt{\frac{\pi}{a}} \exp\left(-\frac{b^2}{4a}\right). \tag{A9}$$

While evaluation of I_y is straightforward, yielding

$$I_y = \sqrt{\frac{\pi}{2(1 + i\tilde{z})}} w(z), \tag{A10}$$

evaluating I_x requires a few more steps: First we separate the generic standing SAW displacement in Eq. (A4) into the sine and cosine quadratures,

$$\cos[K(x - x_0)] = \cos(Kx)\cos(Kx_0) + \sin(Kx)\sin(Kx_0). \tag{A11}$$

Then, since $kA(t) << 1$, we can expand the exponential,

$$\exp\{2ikA(t)\cos[K(x - x_0)]\} \simeq 1 + 2ikA(t)[\cos(Kx)\cos(Kx_0) + \sin(Kx)\sin(Kx_0)]. \tag{A12}$$

Multiplication of this term by the Gaussian function, and their integration, leads to I_x. Since $\sin(Kx)$ is an odd function of x whereas the Gaussian function is even, one integral vanishes and we obtain

$$I_x = I_y + 2ikA(t)\cos(Kx_0) \times \int_{-\infty}^{+\infty} \exp\left[-\frac{2x^2}{w^2(z)}(1 + i\tilde{z})\right] \cos(Kx) \, dx. \tag{A13}$$

We can use the expansion $\cos[Kx] = [\exp(iKx) + \exp(-iKx)]/2$ to obtain the following equation:

$$I_x = I_y + ikA(t)\cos(Kx_0) \times (G^+ + G^-), \quad \text{where}$$
$$G^{\pm} = \int_{-\infty}^{+\infty} \exp\left[-\frac{2x^2}{w^2(z)}(1 + i\tilde{z})\right] \times \exp(\pm iKx) \, dx. \tag{A14}$$

The physical meaning of this equation is the following: For a small SAW displacement A_0, the reflecting surface behaves as an amplitude-diffraction grating with cosine profile. The Gaussian beam impinges on this diffraction grating, and the back reflection is coupled back to the fiber [term I_y in Eq. (A14)]. The diffraction grating also generates two tilted Gaussian beams with angles $\theta^{\pm} = \pm\lambda/\Lambda$, corresponding to the terms G^+ and G^- in Eq. (A14), as will be shown in Sec. III. By using once again the standard integral (A9), we obtain

$$G^{\pm} = \sqrt{\frac{\pi}{2(1 + i\tilde{z})}} w(z) \exp[-B(1 - i\tilde{z})], \tag{A15}$$

where $B = -K^2 w_0^2/8$. Inserting Eq. (A15) into I_x, and I_x into (Eq. (A8)), we get

$$\alpha(z, x_0, t) = \frac{1}{1 + i\tilde{z}}\{1 + 2ikA(t)\cos(Kx_0)\exp[-B(1 - i\tilde{z})]\}. \tag{A16}$$

The amplitude-modulation term is given by $|\alpha(z, t)|^2$, which, after some calculations, can be expressed as

$$|\alpha|^2 = |\alpha|^2_{\text{DC}} + |\alpha|^2_{\Omega}\cos(\Omega t) + |\alpha|^2_{2\Omega}\cos(2\Omega t),$$
$$|\alpha|^2_{\text{DC}} = \frac{1}{1 + \tilde{z}^2},$$
$$|\alpha|^2_{\Omega} = -\frac{2\gamma \times \exp(-B) \times \sin(B\tilde{z})}{1 + \tilde{z}^2}, \tag{A17}$$
$$|\alpha|^2_{2\Omega} = \frac{\gamma^2 \times \exp(-2B)}{1 + \tilde{z}^2},$$

where $\gamma = 2kA_0\cos(Kx_0)$.

APPENDIX B: THE TALBOT EFFECT

Here we explicitly calculate the propagated field after the grating, used to create the plots in Figs. 1 and 5 that visualize the Talbot patterns created by diffraction of a Gaussian beam from a periodic grating. Since the grating affects the propagated field only along the x transverse direction, for simplicity we study the evolution of a one-dimensional (1D) Gaussian beam after reflection from the surface. On the optical axis, we define a new coordinate system $\bar{z}$ with the origin at the surface of the SAW device. In this coordinate system, the beam focus is at position $\bar{z} = z$, where z is the beam defocusing introduced in the calculations for the complex collection ratio. For clarity, and as illustrated in Fig. 5 in the main text, we unfold the reflected field to the right of $\bar{z} = 0$. The field at the surface ($\bar{z} = 0$) is given by the function

$$\psi^{-}_{\text{reflect}}(\bar{z} = 0, x, t) = \psi^{+}_{\text{in}}(z) \times \exp\left[2ikA(t)\cos(Kx_0)\cos(Kx)\right], \tag{B1}$$

where we omitted the sine quadrature in the expansion of the displacement [Eqs. (A4) and (A12)] due to integration in the next step. The field $g(x, \bar{z}, t)$ at a generic position $\bar{z}$ is given by convoluting the input field $\psi^{-}_{\text{reflect}}(\bar{z} = 0, x, t)$ with the impulse response function of free space in the Fresnel approximation (Fresnel-Kirchhoff diffraction integral),

$$h(x, \bar{z}) \simeq h_0 \exp\left(-i\frac{\pi}{\lambda\bar{z}}x^2\right), \tag{B2}$$

where $h_0 = i/(\lambda\bar{z})$, leading to

$$g(x, \bar{z}, t) = h_0 \int_{-\infty}^{+\infty} \psi^{-}_{\text{reflect}}(x', t) \times \exp\left[-i\frac{\pi}{\lambda\bar{z}}(x - x')^2\right] dx'. \tag{B3}$$

Following the same steps that we used to calculate the complex collection ratio $\alpha(z, t)$, we expand the exponential containing the cosine term,

$$\exp\left[i\gamma(t)\cos(Kx)\right] \simeq 1 + i\gamma(t)\cos(Kx), \tag{B4}$$

where $\gamma(t) = 2kA_0\cos(Kx_0)\cos(\Omega t)$. We can expand the cosine in exponential form, $\cos(Kx) = [\exp(iKx) + \exp(-iKx)]/2$, and finally we can rewrite Eq. (B3) as

$$\begin{aligned} g(x, \bar{z}, t) = &\int_{-\infty}^{+\infty} \psi^{+}_{\text{in}} \times h(x - x', \bar{z})\, dx' \\ &+ \frac{i\gamma(t)}{2} \int_{-\infty}^{+\infty} \psi^{+}_{\text{in}} \times e^{iKx'} \times h(x - x', \bar{z})\, dx' \\ &+ \frac{i\gamma(t)}{2} \int_{-\infty}^{+\infty} \psi^{+}_{\text{in}} \times e^{-iKx'} \times h(x - x', \bar{z})\, dx'. \end{aligned} \tag{B5}$$

The first term describes the evolution of a Gaussian beam and therefore represents the back-reflected Gaussian beam, as if it was reflected from a flat surface. The second and third terms describe two tilted beams at an angle of $\theta = \pm\lambda/\Lambda$ with respect to the optical axis, as we can see by writing the second (+) and third (−) terms as

$$g_{\pm} = \frac{i\gamma(t)h_0 C}{2} \exp\left(-\frac{i\pi x^2}{\lambda\bar{z}}\right) \int_{-\infty}^{+\infty} \exp[-ax'^2] \times \exp\left[ix'\frac{2\pi}{\lambda\bar{z}}\left(x \pm \bar{z}\frac{\lambda}{\Lambda}\right)\right] dx', \tag{B6}$$

where

$$a = \left(\frac{1 + iz/z_R}{2w_0^2(1 - z^2/z_R^2)} + \frac{i\pi}{\lambda\bar{z}}\right), \tag{B7}$$

and C is a normalization factor. The integral in Eq. (B5) can be solved by using the standard integral from Eq. (A9). We do not show here the lengthy expression, but an example solution is shown in Fig. 5 in the main text, where we evaluated the integral at $t = 0$ and $z_0 = 5z_T$. As a result of the interference between the diffracted beams, self-images of the field at the grating appear at nonperiodic positions on the optical axis. These positions are dependent on the radius of curvature of the field impinging on the grating, and therefore on the beam defocusing z. Therefore, different values of z lead to different Talbot patterns.

Existence and positions of the self-images

Here we solve Eq. (8) to show that for beam defocusings $z = nz_T$, where n is an integer, one of the self-images is always located at $\bar{z} \simeq -z$. In our coordinate system, with the unfolded reflection, this corresponds to the position of the projection of the image of the fiber. We will also give a proof for Eq. (9).

Starting by substitution of $R_{\bar{z}} = (\bar{z} - z)(1 + z_R^2/(\bar{z} - z)^2)$ into Eq. (8), we obtain a second-order equation $a\bar{z}^2 + b\bar{z} + c = 0$, where $a = z + mz_T/2$, $b = -(mzz_T + z^2 + z_R^2)$, $c = mz_T(z^2 + z_R^2)/2$. This equation has two solutions given by

$$\bar{z}_{1,2} = \frac{m\, z\, z_T + z^2 + z_R^2 \pm \left(z^2 + z_R^2\right)\sqrt{1 - \delta^2}}{2(z + mz_T/2)}, \tag{B8}$$

where $\delta = mz_T z_R/(z^2 + z_R^2)$. The first thing we notice is that the solutions only exist if $\delta^2 \leqslant 1$, which, under the condition that $m > 0$, leads to the equation

$$z_0^2 \geqslant z_R\,(m\, z_T - z_R), \tag{B9}$$

which gives the minimum distance between the beam waist of the focused Gaussian beam and the grating, in order to observe a number m self-images. This equation can be rewritten in terms of the beam radius at the grating, showing that in order to see m self-images, the minimum beam radius at the grating has to be

$$w_{\min}(m) = \Lambda\sqrt{\frac{2m}{\pi}}. \tag{B10}$$

We can now see what happens to Eq. (B8) when $z = nz_T$, in the limit that $\delta \ll 1$, where we can approximate $\sqrt{1 - \delta^2} \simeq 1$,

$$\bar{z}_{1,2} \simeq \frac{m\, n\, z_T^2 + n^2 z_T^2 + z_R^2 \pm \left(n^2 z_T^2 + z_R^2\right)}{z_T(2n + m)}, \tag{B11}$$

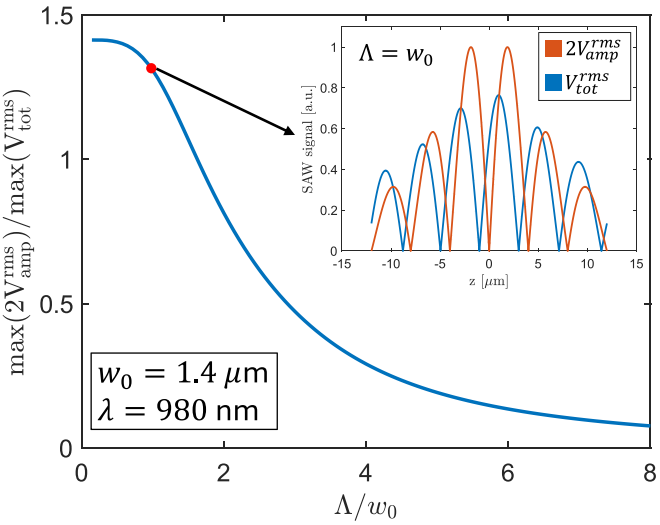

FIG. 6. Ratio $r = \max[2V^{rms}_{amp}(z)]/\max[V^{rms}_{tot}(z)]$, as a function of the acoustic wave Λ. The plot has been calculated from Eqs. (5) and (7), with $w_0 = 1.4$ μm and $\lambda = 980$ nm. Inset: The two signals $2V^{rms}_{amp}(z)$ (red) and $V^{rms}_{tot}(z)$ (blue) for $\Lambda/w_0 = 1$.

and by choosing the solution with the $(-)$ sign, we obtain $\bar{z}_1 \simeq z_T \times mn/(2n+m)$, and for $n = -m$ we get $\bar{z}_1 = -nz_T$, proving that the nth self-image lies at the position $\bar{z} \simeq -z$. To check if $\delta << 1$, we can introduce a variable a equal to the ratio between the SAW wavelength and the beam-waist radius, such that $\Lambda = aw_0$, and we can write

$$\delta = \frac{2\pi\ m\, a^2}{\pi^2 + 4\, m^2 a^4}. \tag{B12}$$

We can see that $\delta \sim m^{-1}$ when $m \to \infty$, and therefore the approximation is better for high values of m. In our experiment, $a = 2$ ($\Lambda = 2.8$ μm and $w_0 = 1.4$ μm), and already for $m = 1$ the approximation used in Eq. (B11) is valid.

APPENDIX C: SAW DETECTION WITH A FIBER CIRCULATOR

An important result of Eqs. (5) and (7) is that under some circumstances, SAW displacements can be better measured without an interferometer. The amplitude-modulation signal can even be larger than the total interferometric signal if we exchange the fiber splitter in Fig. 2 with a fiber circulator. In this way, the optical power is not split in two and the amplitude-modulation signal is twice as big as the amplitude-modulation signal present in the normal interferometric setup. To see this, we choose $w_0 = 1.4$ μm and $\lambda = 980$ nm, and we calculate the ratio $r = \max[2V^{rms}_{amp}(z)]/\max[V^{rms}_{tot}(z)]$, where the factor 2 takes into account the extra optical power available with the fiber circulator. The result is shown in Fig. 6, where it is visible that for $\Lambda/w_0 \lesssim 1.6$, measuring with the fiber circulator leads to a stronger detected signal. We point out that the noise in the two situations is the same since the average optical power impinging on the photodiode is the same. This means that the ratio r also corresponds to the improvement in the signal-to-noise ratio. Finally, we note that Fig. 6 shows the ratio r considering the particular detection scheme used in our experiment, where we have equal optical power in the reference and sample arm of the interferometer (at zero defocusing), and where we lock the interferometer at the side of the fringe. Even under different conditions, our simulations show that there is always an acoustical wavelength such that the $r > 1$, and our claim is still valid.

[1] J. E. Harvey and J. L. Forgham, Am. J. Phys. **52**, 243 (1984).
[2] M. Holler, M. Guizar-Sicairos, E. H. R. Tsai, R. Dinapoli, E. Müller, O. Bunk, J. Raabe, and G. Aeppli, Nature (London) **543**, 402 (2017).
[3] G. Zheng, C. Shen, S. Jiang, P. Song, and C. Yang, Nat. Rev. Phys. **3**, 207 (2021).
[4] J. Miao, Nature (London) **637**, 281 (2025).
[5] W. D. Montgomery, J. Opt. Soc. Am. **57**, 772 (1967).
[6] K. Patorski, in *Progress in Optics*, edited by E. Wolf (Elsevier, Amsterdam, 1989), Vol. 27, pp. 1–108.
[7] J. Wen, Y. Zhang, and M. Xiao, Adv. Opt. Photon. **5**, 83 (2013).
[8] H. Talbot, Lond. Edinb. Dublin Philos. Mag. J. Sci. **9**, 401 (1836).
[9] L. Rayleigh, Lond. Edinb. Dubl. Phil. Mag. J. Sci. **11**, 196 (1881).
[10] L. Rayleigh, Proc. Lond. Math. Soc. **s1-17**, 4 (1885).
[11] M. S. Chapman, C. R. Ekstrom, T. D. Hammond, J. Schmiedmayer, B. E. Tannian, S. Wehinger, and D. E. Pritchard, Phys. Rev. A **51**, R14 (1995).
[12] X.-B. Song, H.-B. Wang, J. Xiong, K. Wang, X. Zhang, K.-H. Luo, and L.-A. Wu, Phys. Rev. Lett. **107**, 033902 (2011).
[13] P. Candelas, J. M. Fuster, S. Pérez-López, A. Uris, and C. Rubio, Ultrasonics **94**, 281 (2019).
[14] A. Bakman, S. Fishman, M. Fink, E. Fort, and S. Wildeman, Am. J. Phys. **87**, 38 (2019).
[15] T. Gao, E. Estrecho, G. Li, O. A. Egorov, X. Ma, K. Winkler, M. Kamp, C. Schneider, S. Höfling, A. G. Truscott, and E. A. Ostrovskaya, Phys. Rev. Lett. **117**, 097403 (2016).
[16] Y. Zhang, J. Wen, S. N. Zhu, and M. Xiao, Phys. Rev. Lett. **104**, 183901 (2010).
[17] G. G. Rozenman, W. P. Schleich, L. Shemer, and A. Arie, Phys. Rev. Lett. **128**, 214101 (2022).
[18] S. G. Joshi and R. M. White, J. Acoust. Soc. Am. **46**, 17 (1969).
[19] A. Mamishev, K. Sundara-Rajan, F. Yang, Y. Du, and M. Zahn, Proc. IEEE **92**, 808 (2004).
[20] R. M. White and F. W. Voltmer, Appl. Phys. Lett. **7**, 314 (1965).
[21] P. Delsing, A. N. Cleland, M. J. A. Schuetz, J. Knörzer, G. Giedke, J. I. Cirac, K. Srinivasan, M. Wu, K. C. Balram, C. Bäuerle, T. Meunier, C. J. B. Ford, P. V. Santos, E. Cerda-Méndez, H. Wang, H. J. Krenner, E. D. S. Nysten, M. Weiß, G. R. Nash, L. Thevenard *et al.*, J. Phys. D: Appl. Phys. **52**, 353001 (2019).
[22] K. Yamanouchi, Y. Cho, and T. Meguro, *IEEE 1988 Ultrasonics Symposium Proceedings* (IEEE, Chicago, IL, USA, 1988), pp. 115–118, Vol. 1.

[23] S. Büyükköse, B. Vratzov, J. van der Veen, P. V. Santos, and W. G. van der Wiel, Appl. Phys. Lett. **102**, 013112 (2013).
[24] L. Wang, S. Chen, J. Zhang, J. Zhou, C. Yang, Y. Chen, and H. Duan, Appl. Phys. Lett. **113**, 093503 (2018).
[25] L. Shao, S. Maity, L. Zheng, L. Wu, A. Shams-Ansari, Y.-I. Sohn, E. Puma, M. N. Gadalla, M. Zhang, C. Wang, E. Hu, K. Lai, and M. Lončar, Phys. Rev. Appl. **12**, 014022 (2019).
[26] M. J. A. Schuetz, E. M. Kessler, G. Giedke, L. M. K. Vandersypen, M. D. Lukin, and J. I. Cirac, Phys. Rev. X **5**, 031031 (2015).
[27] M. E. Msall and P. V. Santos, Phys. Rev. Appl. **13**, 014037 (2020).
[28] R. Takasu, Y. Sato, T. Hata, T. Akiho, K. Muraki, and T. Fujisawa, Appl. Phys. Express **12**, 055001 (2019).
[29] T. Luschmann, A. Jung, S. Geprägs, F. X. Haslbeck, A. Marx, S. Filipp, S. Gröblacher, R. Gross, and H. Huebl, Mater. Quantum. Technol. **3**, 021001 (2023).
[30] R. Manenti, M. J. Peterer, A. Nersisyan, E. B. Magnusson, A. Patterson, and P. J. Leek, Phys. Rev. B **93**, 041411(R) (2016).
[31] E. B. Magnusson, B. H. Williams, R. Manenti, M.-S. Nam, A. Nersisyan, M. J. Peterer, A. Ardavan, and P. J. Leek, Appl. Phys. Lett. **106**, 063509 (2015).
[32] B. A. Moores, L. R. Sletten, J. J. Viennot, and K. W. Lehnert, Phys. Rev. Lett. **120**, 227701 (2018).
[33] M. Fisicaro, T. A. Steenbergen, Y. C. Doedes, K. Heeck, and W. Löffler, Phys. Rev. Appl. **23**, 014032 (2025).
[34] S. Szapiel and K. Patorski, Optica Acta: Intl. J. Optics **26**, 439 (1979).